J Mol Model (2011) 17:2375–2383
DOI 10.1007/s00894-011-0981-z

ORIGINAL PAPER

Application of a SCC-DFTB QM/MM approach to the investigation of the catalytic mechanism of fatty acid amide hydrolase

Luigi Capoferri · Marco Mor · Jitnapa Sirirak · Ewa Chudyk · Adrian J. Mulholland · Alessio Lodola

Received: 4 December 2010 / Accepted: 21 January 2011 / Published online: 2 March 2011

Abstract Self-consistent charge density functional tight binding (SCC-DFTB) is a promising method for hybrid quantum mechanics/molecular mechanics (QM/MM) simulations of enzyme-catalyzed reactions. The acylation reaction of fatty acid amide hydrolase (FAAH), a promising drug target, was investigated by applying a SCC-DFTB/CHARMM27 scheme. Calculated potential energy barriers resulted in reasonable agreement with experiments for oleamide (OA) and oleoylmethyl ester (OME) substrates, outperforming previous calculations performed at the PM3/CHARMM22 level. Furthermore, the experimental preference of FAAH in hydrolyzing OA faster than OME was adequately reproduced by calculations. All these findings indicate that the SCC-DFTB/CHARMM27 approach can be successfully applied to mechanistic investigations of FAAH-catalyzed reactions.

Keywords QM/MM · SCC-DFTB · FAAH · Reaction mechanism · Computational enzymology

L. Capoferri · M. Mor · A. Lodola (✉)
Dipartimento Farmaceutico, Università degli Studi di Parma,
viale G. P. Usberti 27/A Campus Universitario,
43124 Parma, Italy
e-mail: Alessio.Lodola@unipr.it

J. Sirirak · E. Chudyk · A. J. Mulholland (✉)
Centre for Computational Chemistry School of Chemistry,
University of Bristol,
Bristol BS8 1TS, UK
e-mail: Adrian.Mulholland@bristol.ac.uk

Introduction

Mechanistic simulations of enzyme-catalyzed reactions within a realistic environment (composed of a full protein structure and solvent molecules) are made possible by the application of hybrid quantum mechanics/molecular mechanics (QM/MM) methods [1]. In the QM/MM framework, the simulation system (e.g., the enzyme–substrate complex) is divided into two linked regions: (i) the core (QM) region which contains the reacting fragments and it is described by quantum mechanics; (ii) the surrounding protein, represented by a molecular mechanics force field [2, 3]. In this way, it is possible to treat systems composed by thousand of atoms and to describe the potential energy surfaces (PESs) relevant to enzymatic chemistry [4, 5]. In the QM/MM approach, the reactive region of the enzyme's active site can be treated with one of the available QM techniques, such as semiempirical methods, density functional theory (DFT), or ab initio molecular orbital methods [6].

Accurate results (near to the so-called "chemical accuracy" in the best cases) can be obtained (e.g., for energy barriers) when the QM/MM method employed is based on ab initio electron correlation approaches such as the MP2 perturbation method and coupled-cluster theory [7, 8]. Unfortunately, these methods are very computationally demanding, and this limits their application to energy minimization/geometry optimization for small QM regions or "single point" calculations on structures optimized at lower levels. On the other hand, semiempirical molecular orbital techniques, while not suitable for all systems, allow large QM regions to be treated and more extensive simulations to be performed (e.g., testing alternative

reaction mechanisms or exploring multiple reaction paths [9]) at the cost of limited accuracy in reproducing experimental data [10].

An attractive alternative to ab initio and traditional semiempirical methods (e.g., AM1 or PM3) within the context of hybrid QM/MM simulations is represented by the self-consistent charge density functional tight binding (SCC-DFTB) method [11, 12]. The SCC-DFTB has proven to be excellent for geometries and to perform well for many biomolecular systems [13]; in the best cases, it has performed as well as DFT calculations based on hybrid functionals [14]. Furthermore, since its implementation in widely used QM/MM packages such as CHARMM [15] and AMBER [16], SCC-DFTB has become increasingly widely applied in QM/MM calculations, and has been found in some cases to give results that are in good agreement with QM/MM calculations performed at higher levels of theory [15]. SCC-DFTB is a more modern method, and has only more recently become available for QM/MM calculations, so it has been used less extensively than earlier semiempirical molecular orbital methods for enzyme reaction modeling. Thus, its reliability in this field is rather less well tested [17].

In recent years, we have elucidated the mechanisms of reaction [18] and inhibition [19] of fatty acid amide hydrolase (FAAH) [20], a serine hydrolase of pharmaceutical interest [21], by means of QM/MM simulations based on the PM3 Hamiltonian. PESs of the modeled reactions were initially built at the PM3/CHARMM level, and the energetics were corrected with DFT single-point calculations to overcome the known limits of PM3. Although this approach has been shown to give reliable results in many cases [1], it has some explicit drawbacks: (i) it is computationally demanding, as hundreds of single-point DFT calculations are required [22]; (ii) it relies on the assumption that DFT methods are relatively insensitive to the quality of the geometry of the system under consideration, which may not always be the case.

FAAH has become an important model system in the field of QM/MM enzyme reaction modeling. Its catalytic mechanism is now well understood thanks to computational works done by different research groups [18, 23]. For validation purposes, it is fundamental that independent simulations (e.g., different QM/MM techniques) arrive at similar mechanistic conclusions.

In this context, the availability of a DFTB-based QM/MM potential, which may retain DFT-type accuracy [7] at a reduced computational cost, prompted us to test its performance in the case of FAAH. We therefore investigated the acylation reaction of FAAH with oleamide (OA) and oleoylmethyl ester (OME) substrates by applying the SCC-DFTB/CHARMM27 QM/MM potential implemented in the CHARMM program (version CHARMM30b2) [24]. We calculated PESs for the reactions for multiple starting structures and compared with our previous calculations at the PM3/CHARMM22 and B3LYP/6-31+G(d)//PM3/CHARMM22 levels of theory [18]. Our previous work has shown the importance of considering multiple conformations in QM/MM mechanistic modeling. The work reported here shows that SCC-DFTB/CHARMM27 significantly outperforms calculations on FAAH with semiempirical molecular orbital methods. The SCC-DFTB/CHARMM27 energy barriers are in reasonable agreement with those derived from experimental kinetics, and in significantly better agreement than those calculated at the PM3/CHARMM22 level. More importantly, the remarkable (experimentally observed [25]) preference of FAAH in hydrolyzing the amide (OA) faster than the ester (OME) is satisfactorily reproduced by the SCC-DFTB/CHARMM27 protocol applied here.

Methods

Application of the QM/MM potential for reaction modeling

We applied the SCC-DFTB/CHARMM27 QM/MM method to model the acylation reaction of FAAH. The quantum mechanical region included in the calculations (Fig. 1) was relatively large (34 atoms for OA, 36 for OME), similar to the region investigated in our previous work [18]. It includes the methylamine group of Lys142, the side chains of Ser217 and Ser241, and the butanamide fragment for OA as well as the butanoyl methyl ester one for OME. All the other atoms of the system were treated with the CHARMM27 MM force field [26, 27]. For the water molecules, the CHARMM variant of the TIP3P model (TIPS3P) was used [28, 29]. The covalent bonds

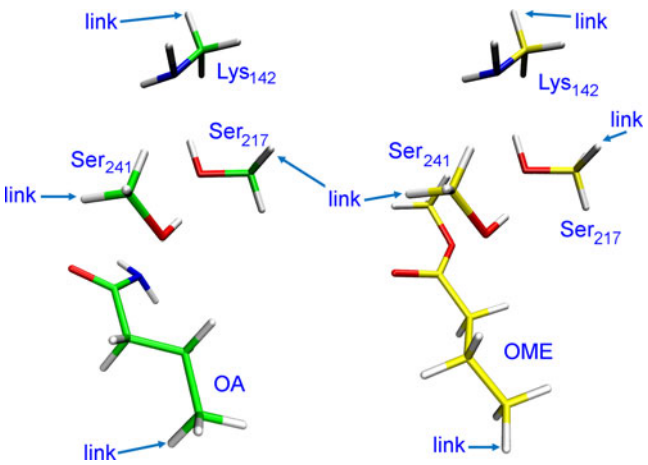

Fig. 1 The QM regions employed in the QM/MM simulations with OA (*left*, *green carbons*) and OME (*right*, *yellow carbons*). "Link" atoms [15] are indicated

crossing the boundary between the QM and MM regions were treated by introducing four "HQ" link atoms which are included in the QM system. The QM/MM approach used here includes bonded and nonbonded interactions between the QM and MM systems and accounts for the essential effect of the protein on the modeled reactions [15]. Van der Waals and bonded interactions were described by MM terms, with standard CHARMM27 parameters used for the QM atoms. Electrostatic interactions were treated by calculating the Coulombic interactions between the Mulliken charges of the QM atoms and the MM partial atomic charges [15]. A group-based nonbonded cut-off of 12 Å was applied and atoms further than 14 Å from the Ser241 hydroxyl oxygen were fixed. With the exception of these boundary restraints, all the other atoms were free to move during the calculations.

Model building

The Cartesian coordinates of the reactants (Michaelis complexes) were taken from those used in our previous studies [18, 30], which were based on the crystal structure of rat FAAH in its covalent adduct with methyl arachidonyl phosphonate [31]. The FAAH-OA and FAAH-OME complexes were first minimized to an energy gradient of 0.01 kcal mol^{-1} $Å^{-1}$ by applying the SCC-DFTB/CHARMM27 potential and thus equilibrated by stochastic boundary molecular dynamics (SBMD) [32].

The SCC-DFTB/CHARMM27 potential was used to generate a trajectory using a time step of 1.0 fs for the integration, and a cut-off distance for nonbonded interactions of 12 Å. During the simulation, all atoms further than 21 Å away from the center of the sphere (Ser241 O_1) were harmonically restrained to their crystallographic coordinates with force constants based on model average beta-factors [33]. Frictional coefficients of 250 ps^{-1} for non-hydrogen protein atoms and 62 ps^{-1} on water oxygen atoms were applied at a buffer region, and a deformable boundary potential was also applied for the water oxygens.

The simulation was divided into three phases: (i) a heating phase of 100 ps to increase the temperature from 0 to 300 K; (ii) an equilibration phase of 200 ps at 300 K; (iii) a production phase of 150 ps at 300 K.

One snapshot every 25 ps of the SCC-DFTB/CHARMM27 MD production phase was considered for the modeling investigation, to give a total of six equally spaced starting structures. The equilibrated structures were newly minimized and thus employed for mechanistic QM/MM calculations. For both OA and OME, the minimum energy pathway with the lowest energy barriers was found with the Michaelis complex obtained after 75 ps of the MD production phase.

Calculation of potential energy surfaces

Reaction coordinates were defined for every reaction step and restrained sequentially to move the system along a given reaction path. Distance-dependent reaction coordinate restraints [34] were applied using the RESD command of CHARMM [24]. A force constant of k=5000 kcal mol^{-1} $Å^{-2}$ was used to restrain all the defined coordinates. The values for the restrained distances were increased continuously to force the system across the barrier of a specific reaction step. Energy minimizations (by ABNR) of all structures were performed to a gradient tolerance of 0.01 kcal mol^{-1} $Å^{-1}$. The structures of energy minima (i.e., stable structures) were determined more precisely by performing additional geometry optimizations with none of the reaction coordinates restrained. The final energy of a structure (as indicated on the potential energy surfaces, for example) was obtained by performing single-point energy calculations where the energy contribution derived from any restraint was left out. The potential energy surfaces are useful for the determination of basic mechanistic features such as the identification of transition states and intermediates, or as an indication of the concertedness of the modeled reaction [35, 36]. However, it should be remembered that the PESs reported here do not include the zero-point energy nor the influence of hydrogen tunneling effects that may affect the effective barriers to the reaction.

Results and discussion

FAAH is endowed with a Lys142–Ser217–Ser241 catalytic triad [37] that is responsible for its notable ability to hydrolyze amides faster than esters through a mechanism in which acylation is rate-limiting [38]. The mechanism of hydrolysis catalyzed by FAAH is widely accepted, with Lys142 serving as a key acid and base in distinct steps of the catalytic cycle [39]. As a base, Lys142 activates the Ser241 nucleophile for attack on the substrate amide carbonyl (Fig. 2). As an acid, Lys142 readily protonates the substrate leaving group leading to its expulsion. The impact of Lys142 on Ser241 nucleophile strength and leaving group protonation occurs indirectly, via the bridging Ser217 of the triad, which acts as a "proton shuttle."

The mechanism described above was explored by means of the adiabatic mapping approach, which has already been shown to work well with this and other systems [40]. As shown in Fig. 2, the reaction was modeled in three main steps starting from the FAAH–OA and FAAH–OME Michaelis complexes: (I) formation of the TI; (IIa) leaving group protonation; (IIb) leaving group expulsion and formation of the acylated Ser241. A similar strategy has

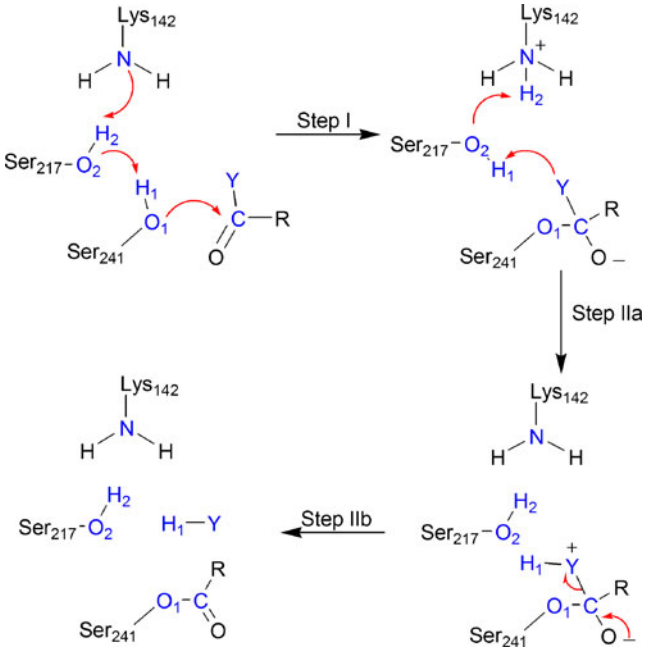

Fig. 2 Acylation mechanism of FAAH [30] in the presence of oleamide (OA) and for oleoylmethyl ester (OME). *Y* is $-NH_2$ for OA (the label N_{am} is used for its nitrogen leaving group in the text), and $-OCH_3$ for OME (O_{es} is used as a label for its oxygen leaving group in the text). Labels are also consistent with the definition of the reaction coordinates employed in the calculations

been successfully applied to model the reaction between FAAH and carbamate inhibitors [19].

Step I of the acylation reaction consists of multiple events: a proton is abstracted from Ser241 and, via the bridging residue Ser217, transferred to the general base Lys142. Thus, the activated Ser241 attacks the carbonyl group of the substrate, leading to the formation of the TI.

With this in mind, step I of the acylation was modeled by restraining the following two reaction coordinates: *Rx*, defined as $[d(O_1, H_1) - d(O_2, H_1) - d(O_1, C)]$, including proton abstraction from Ser241 by Ser217 and nucleophilic attack by Ser241; and *Ry*, defined as $[(dO_2, H_2)] - d[(N, H_2)]$, which describes the proton transfer between Ser217 and Lys142. *Rx* and *Ry* were increased in steps of 0.15 Å and 0.1 Å, respectively, with harmonic restraints of 5000 kcal mol^{-1} $Å^{-2}$ (similar to the approach used in [18, 19]).

Step II of the acylation reaction was simulated by employing the adiabatic mapping approach. The modeling of acylenzyme formation from the TI was separated into two sub-events: the protonation of the leaving group (a), and its consequent expulsion (b).

In the case of OA, step IIa was modeled using the following reaction coordinates: *Rt*, defined as the difference between atomic distances $[d(O_2, H_1) - d(N_{am}, H_1)]$ upon moving the proton H_1 from Ser217 to N_{am} of OA; and *Rs*, defined as $[d(N, H_2) - d(O_2, H_2)]$ upon moving proton H_2 from Lys142 back to Ser217.

Step IIb was explored by restraining *Rr*, which is defined as $[d(N_{am},C)]$ and describes the scission of the bond between the carbonyl carbon and the amide nitrogen. *Rt*, *Rs* and *Rr* were increased in steps of 0.1 Å with harmonic restraints of 5000 kcal mol^{-1} $Å^{-2}$.

A similar approach was employed to model the second step of FAAH acylation in the presence of OME, with the following differences. In step IIa, the protonation of the leaving group involved the alcoholic oxygen O_{es} and was thus described by *Rt* as $[d(O_2, H_1) - d(O_{es}, H_1)]$. In step IIb, the expulsion of leaving group requires the breaking of a C–O bond and was thus modeled using $[d(O_{es},C)]$ as the reaction coordinate.

In the present study, different snapshots were taken from the SCC-DFTB/CHARMM27 MD simulations and used as starting points for modeling FAAH acylation. The reaction energetics reported here refer to the FAAH-OA and FAAH-OME Michaelis complexes that give the lowest potential energy barriers. However, alternative starting points gave similar pathways and barriers (vide infra). Thus, the PESs and geometries presented here can be regarded as being representative of the modeled reactions.

The SCC-DFTB/CHARMM27 PESs of FAAH acylation in the presence of OA are reported in Fig. 3. The surface relative to step I is reported in the left panel. The change in energy during Ser241 deprotonation and subsequent nucleophilic attack can be followed along *Rx*, while the change in the energy during the protonation of Lys142 can be observed along *Ry*. The minimum energy path (MEP) connecting the Michaelis complex (A) to the tetrahedral intermediate (TI, C) on the SCC-DFTB/CHARMM27 surface shows the presence of a concerted process, similar to what was observed in our previous B3LYP/6-31+G(d)//PM3/CHARMM22 calculations. It is worth noting that the SCC-DFTB/CHARMM22 step I has an energy barrier of 16.1 kcal mol^{-1}. This barrier is in good agreement with that calculated with B3LYP/6-31+G(d)//PM3/CHARMM22 (18.0 kcal mol^{-1}), and it is significantly smaller than that calculated at the PM3/CHARMM22 level of theory (36.0 kcal mol^{-1}) [18]. It is also worth noting that the SCC-DFTB/CHARMM27 PES resembles the B3LYP/6-31+G(d)//PM3/CHARMM22 surface much more than the PM3/CHARMM22 one reported in [18]. In particular, while a shallow minimum area was identified around *Rx*=−3.0, *Ry*=0.4 of the PES at the PM3-CHARMM22 level [18], no minima was found in the corresponding area at both the B3LYP/6-31+G(d)//PM3/CHARMM22 [18] and SCC-DFTB/CHARMM27 levels. Taken together, these findings indicate that SCC-DFTB reproduces B3LYP potential energy values fairly well, at least for the reaction under investigation.

Visual inspection of the approximate TS (B) indicates that it is associated with Ser241 activation, with proton H_1

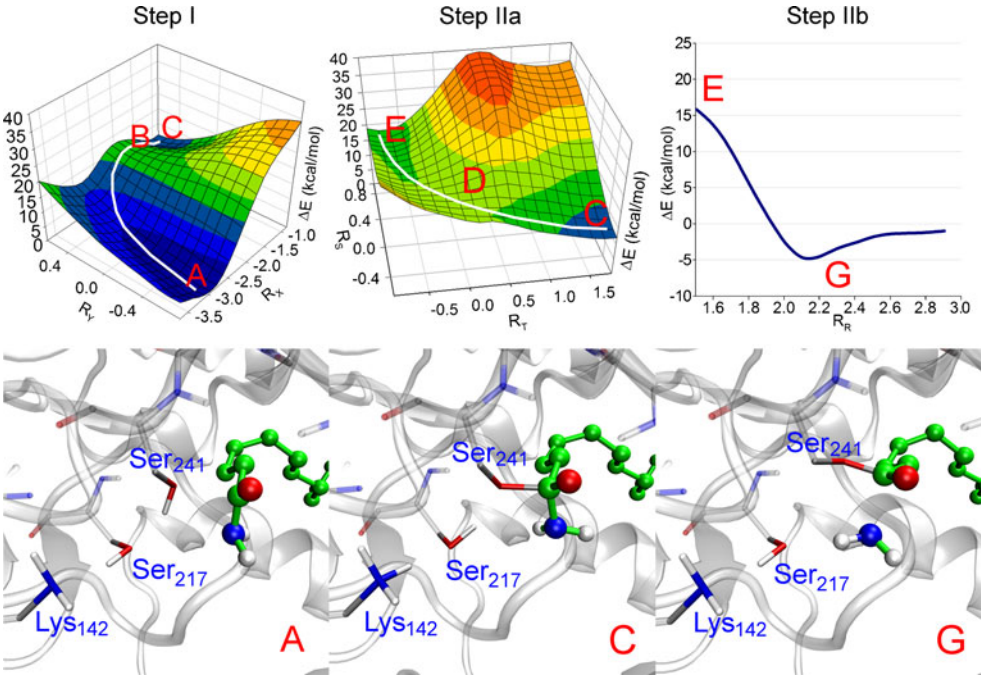

Fig. 3 SCC-DFTB/CHARMM27 QM/MM PESs (*top*) for FAAH acylation in the reaction with OA. The structures of some configurations are also shown: *A* (Michaelis complex), *C* (tetrahedral intermediate), *G* (acylenzyme). FAAH active site residues are represented by *white carbon atoms*, while OA carbons are *green*

being transferred from O_1 to O_2 (Table 1), similar to what was observed at the other levels of theory [18]. Conversely, at the TS, the proton transfer involving Ser217 and Lys142 is nearly complete (the N–H_2 distance is 1.1 Å), while the nucleophilic attack is only just starting, as the O_1–C distance is close to the value observed in the Michaelis complex. Even though the predicted TS involves proton transfer rather than nucleophilic attack, the absence of an energy barrier between B and C indicates that Ser241 deprotonation and nucleophilic attack are effectively concerted.

The product of step I, the TI, is less stable than the Michaelis complex by 11.5 kcal mol^{-1}, indicating its transient character. On the other hand, this configuration is greatly stabilized by the FAAH oxyanion hole (omitted from Fig. 3 for clarity), which forms hydrogen bonds with the negatively charged oxygen of the substrate, as also reported in previous calculations [18, 23]. Interestingly, a water molecule (conserved in FAAH [41]) was found to interact with the carbonyl oxygen of OA in both the TS and TI, assisting the stabilization of the incoming negative charge on the oxygen atom.

Visual inspection of the TI structure confirms the presence of a new bond between Ser241 O_1 and the carbonyl carbon of OA (O_1–C=1.62 Å), as well as the presence of a protonated and positively charged Lys142 (N–H_1=1.07 Å) at the active site. Furthermore, in the TI leaving group, the N_{am} atom is correctly oriented towards the hydroxyl group of Ser217 to initiate the second step of the acylation (Fig. 3, lower middle panel). This finding differs from what was observed at the PM3/CHARMM22 level, where a rearrangement of the TI due to the pyramidal inversion of N_{am} was required to start step II [30].

The SCC-DFTB/CHARMM27 PES associated with step IIa is reported in the central panel of Fig. 3. The change in energy during the protonation of the basic nitrogen of OA (N_{am}) by Ser217 can be followed along *Rt*, while the change in energy during the transfer of H_2 from Lys142 to Ser217 can be observed along *Rs*. The MEP identified on the surface showed a mechanism where the protonation of the basic nitrogen of OA (N_{am}) by Ser217 is almost completed before the transfer of H_2 from Lys142 to Ser217 has begun. However, as this second event takes place with no barrier, the double proton transfer of step IIa can be considered a concerted process. These events lead to configuration E, which requires surmounting a barrier of 18.8 kcal mol^{-1} (relative to the Michaelis complex), ~3 kcal mol^{-1} higher than that calculated here for the deprotonation of Ser241.

Visual inspection of the approximate TS structure E shows H_1 being transferred from O_2 to N_{am}, (N_{am}-H_1=1.19 Å; O_2–H_1=1.37 Å), suggesting that leaving group protonation is the rate-liming event for FAAH acylation. The activation barrier of 18.8 kcal mol^{-1} is in good agreement with the experimentally deduced one of 16.0 kcal mol^{-1}, and significantly smaller than that calculated at the PM3/CHARMM22 level (40.0 kcal mol^{-1} [30]). As a consequence of the protonation of N_{am}, configuration E is characterized by a slightly longer C–N_{am} bond and a shorter O_1–C than that observed in the TI (Table 1).

Step IIb occurs with no barrier (Fig. 3, right panel), leading to the formation of the acylenzyme G. Protonation and the expulsion of the leaving group (i.e., neutral ammonia) are thus highly concerted. The acylenzyme is characterized by a planar carbonyl bond and by a short

Table 1 Distances between reactant atoms (Å). Atom labels are consistent with Fig. 2

	O1···C		O1···H1		O2···H1		O2···H2		N···H2		C···Y		Y···H1	
	OA	OME	OA	OME	OA	OME	OA	OME	OA	OME	OA	OME	OA	OME
A	2.18	2.13	0.99	1.01	1.76	1.73	1.00	1.01	1.97	1.91	1.39	1.39	2.45	2.35
B	2.04	1.87	1.41	1.54	1.25	1.16	1.63	1.45	1.09	1.15	1.41	1.46	2.96	2.45
C	1.62	1.59	1.66	1.72	1.03	1.03	1.71	1.68	1.07	1.07	1.46	1.50	2.81	2.21
D	1.49	1.49	2.48	2.26	1.37	1.50	1.40	1.14	1.17	1.44	1.50	1.51	1.19	1.06
E	1.49	1.48	2.35	2.22	1.70	1.75	1.01	1.01	1.88	1.91	1.51	1.51	1.07	1.01
G	1.38	1.35	2.60	2.49	1.90	1.82	1.01	1.01	1.89	1.89	2.11	2.41	1.04	1.00

O_1–C distance (1.38 Å), while the ammonia group remains quite close to Ser217 even after its expulsion (Fig. 3, lower right panel). Finally, G is calculated to be more stable than the Michaelis complex by 4.7 kcal mol^{-1}, indicating an exothermic overall profile. This is similar to what was found at the B3LYP/6-31+G(d)//PM3/CHARMM22 level of theory, where G was more stable than the reactants by 1.8 kcal mol^{-1} (unpublished data).

The acylation mechanism of FAAH in the presence of OME substrate was modeled by applying the same procedure as described for OA. The SCC-DFTB/CHARMM27 PESs for FAAH acylation by OME are reported in Fig. 4. The PES for step I, explored by applying the reaction coordinates *Rx* and *Ry*, is reported in the left panel of the same figure. The MEP connecting the Michaelis complex (A) and the TI (C) is similar to that observed for OA. The energy barrier required for the formation of the TI (C) is 18.9 kcal mol^{-1} relative to the substrate complex A, significantly lower than that calculated at the PM3/CHARMM22 level (44 kcal mol^{-1} [30]).

The examination of the approximate TS geometry (B) shows that Ser241 deprotonation is the crucial event of the first step in acylation. However, the proton transfer of H_1 to Ser217 O_2 is more advanced than it is for OA (Table 1). Ser241 deprotonation and the subsequent nucleophilic attack are tightly coupled, as no barrier is found between B and C. Although stabilized by the oxyanion hole, the TI (C) is less stable than the Michaelis complex by 12.5 kcal mol^{-1}. Unlike what is observed for OA, in configurations B and C no water molecule is found to interact with the carbonyl oxygen of OME. Visual inspection of the FAAH-OME and FAAH-OA TI structures suggests that the methoxy group of OME actually displaces this important water molecule. The lack of an additional hydrogen bond can thus account for the slightly higher barrier found in the first step of FAAH acylation by OME.

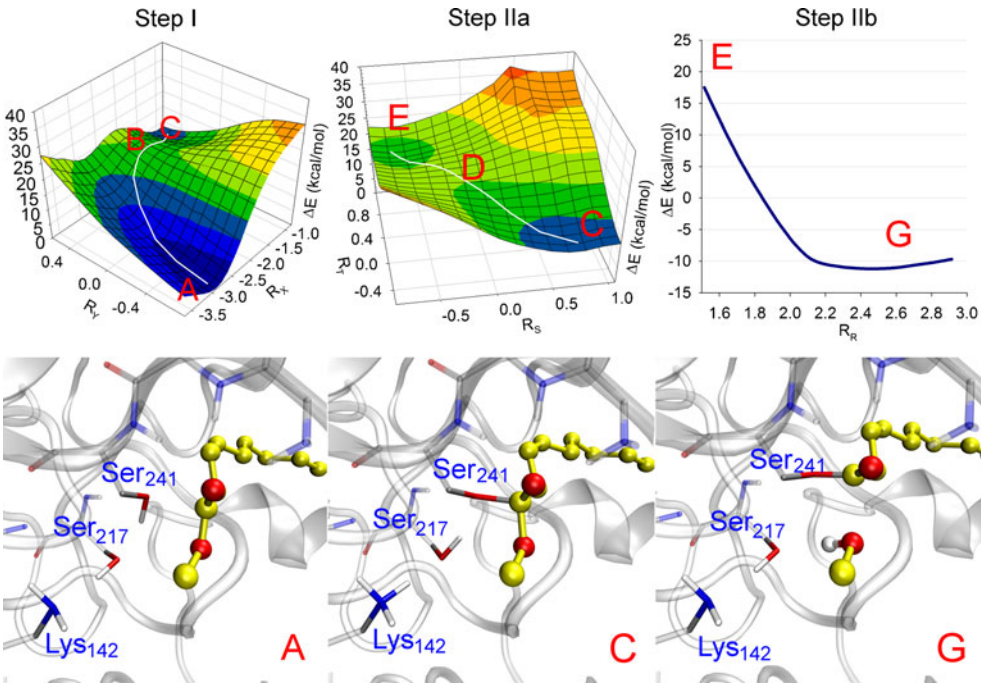

Fig. 4 SCC-DFTB/CHARMM27 QM/MM PESs for FAAH acylation in the reaction with OME (oleoylmethyl ester). The geometry-relevant configurations are also reported: *A* (Michaelis complex), *C* (tetrahedral intermediate), *G* (acylenzyme). FAAH active site residues are represented by *white carbon atoms*, while OME carbons are *yellow*

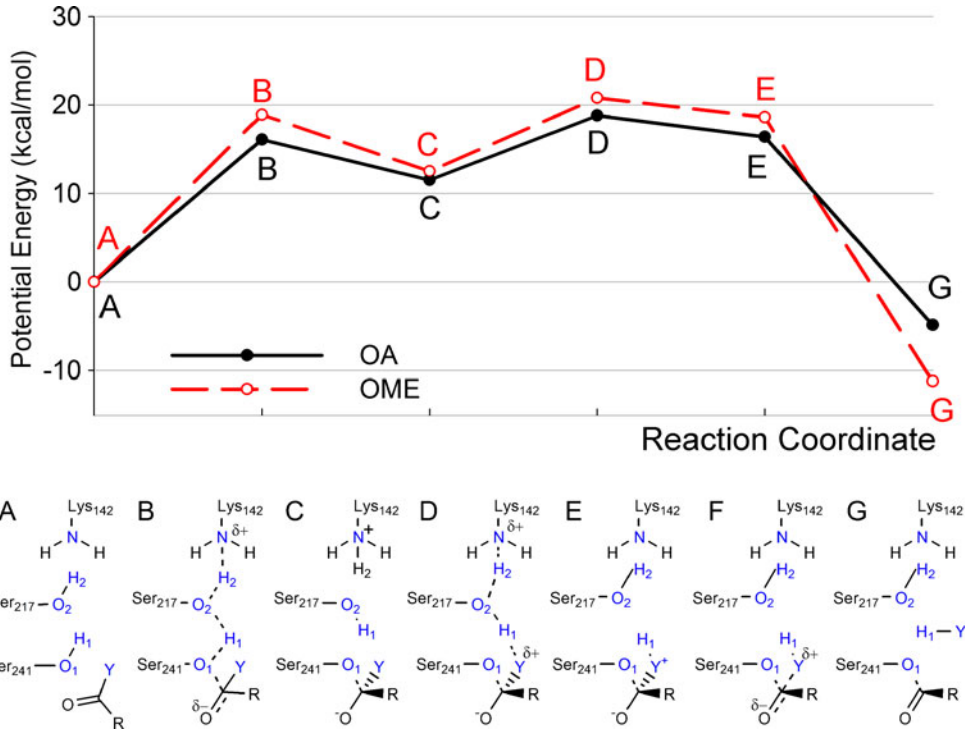

Fig. 5 SCC-DFTB/CHARMM27 QM/MM potential energy profiles for FAAH acylation by OA (*solid line*) and OME (*dashed line*). The relevant configurations are: the Michaelis (substrate) complex (*A*), TS for TI formation (*B*), TI (*C*), TS for leaving group protonation (*D*), protonated TI (*E*), and acylenzyme (*G*)

The subsequent formation of the acylenzyme from the TI is again a complex multiproton-transfer process. The SCC-DFTB/CHARMM27 PES associated with step IIa is reported in the central panel of Fig. 4.

The highest-energy point along the MEP (D) is the TS for the protonation of the leaving group oxygen (O_{es}). This process leads to E overcoming a barrier of 20.8 kcal mol^{-1} relative to the substrate complex A. Calculation at the PM3/CHARMM22 level predicted an energy barrier of 47.0 kcal mol^{-1} for step IIa [30].

The subsequent expulsion of methanol happens spontaneously, as there is effectively no energy barrier between E and the acylenzyme G. Also in this case, G is calculated to be more stable than the Michaelis complex (by 11.0 kcal mol^{-1}), indicating the presence of an exothermic profile overall.

Figure 5 summarizes the potential energy profiles for acylation of FAAH in the presence of OA and OME at the SCC-DFTB/CHARMM27 level. The calculations indicate that these substrates follow a similar mechanism of FAAH acylation, with the collapse of TI being the rate-limiting step of the process.

The calculated barrier (relative to A) to amide cleavage is 18.8 kcal mol^{-1}, 2.0 kcal mol^{-1} smaller than the barrier to the ester. These findings are in agreement with kinetic investigations of OA and OME substrates [25, 28]: the experimental barrier to the hydrolysis of oleamide is ~1 kcal mol^{-1} lower than that for oleoylmethyl ester. The calculations suggest that this unique preference for the amide depends on both the more efficient stabilization of the TS for the deprotonation of Ser241 and the higher basicity of the nitrogen N_{am} compared to that of the oxygen O_{es} in the TI.

As QM/MM calculations based on adiabatic mapping along a reaction coordinate may hide potential pitfalls due to conformational transitions at the protein's active site [42], the SCC-DFTB/CHARMM27 calculations were repeated for other starting conformations of FAAH in complex with the two considered substrates.

Five additional FAAH-OA and FAAH-OME Michaelis complexes were extracted from the MD trajectory (see the "Methods" section) and employed to build PESs for the acylation reaction. The same adiabatic mapping protocol described above was employed to drive the systems from

Table 2 SCC-DFTB/CHARMM27 energy values (kcal mol^{-1}) for key configurations (B, C, and D) obtained by simulating FAAH acylation in the presence of OA and OME using different Michaelis complexes (structures 1–6)

Structure	B (TS1)		C (TI)		D (TS2)	
	OA	OME	OA	OME	OA	OME
1	18.8	19.6	12.6	11.1	23.3	25.3
2	17.6	20.4	11.2	12.7	21.0	25.2
3	16.1	18.9	11.5	12.5	18.8	20.8
4	18.5	20.8	11.5	13.3	20.3	25.6
5	16.8	20.1	10.9	13.2	19.8	24.7
6	18.8	22.0	12.0	15.7	23.4	26.4
Mean	17.8	20.3	11.6	13.1	21.1	24.7
Mean SE	0.5	0.4	0.2	0.6	0.8	0.8

the reactants to the products. Although the PESs and the relative positions of the stationary points were not affected by the geometry of the starting points, small differences were observed in the energies of key stationary points.

The results of these calculations are summarized in Table 2, where energy values of TSs and TIs are also reported as mean values together with the corresponding standard errors of the mean (mean SE). The energy values are consistent with those reported in Fig. 5, confirming that TI collapse controls the reaction rate of FAAH acylation for both OA and OME. The key energy barrier to OA acylation is also lower than that for OME when multiple starting conformations are considered, suggesting that a difference of 2–3 kcal mol^{-1} between energy barriers can be considered to be significant at this level of theory, as long as sufficient conformations are investigated.

Analysis of the data reveals that at the SCC-DFTB/CHARMM27 level too, conformational fluctuations of the active site of FAAH affect calculated barriers, and may be important for an efficient catalytic process [9]. For OA, the activation barriers of the main TS (configuration D) differ significantly between the six simulations, with an absolute range of variation of 4.6 kcal mol^{-1} (calculated as the difference between the highest and lowest E_{act} obtained). This is also the case for OME, with an absolute range of variation of 5.6 kcal mol^{-1} (for configuration D). Further investigations, similar to those reported in [9], will be required to unravel the effects of active-site fluctuations on FAAH-catalyzed reactions at the SCC-DFTB/CHARMM27 level of theory.

Conclusions

We evaluated the performance of a SCC-DFTB/CHARMM27 method by modeling the mechanism of a well-known enzyme-catalyzed reaction, the acylation of FAAH in the presence of OA and OME substrates.

The results support the previously proposed mechanism [18, 30]. Indeed, the exploration of the PESs for FAAH acylation indicates that the collapse of the tetrahedral intermediate is the rate-limiting step of the reaction for both OA and OME substrates, with calculated barriers of 18.8 and 20.8 kcal mol^{-1}, in good agreement with the experimentally deduced ones of 16.0 and 17.0 kcal mol^{-1}. Also, if the SCC-DFTB/CHARMM27 energy values are averaged over multiple reaction paths, the resulting potential energy barriers (21.1±0.8 kcal mol^{-1} for OA and 24.7±0.8 kcal mol^{-1} for OME) are in reasonable agreement with experimental observations.

It should be remembered that the PESs obtained here do not include zero-point energy nor the influence of hydrogen tunneling effects, which may lower the calculated barriers by a few kcal mol^{-1} [43]. Regardless of the possible role played by quantum effects in FAAH catalysis, the SCC-DFTB/CHARMM27 activation barriers are significantly lower than those calculated at the PM3/CHARMM22 [18, 30] and PDDG-PM3/OPLS [23] levels previously reported in the literature. In this respect, the SCC-DFTB/CHARMM27 method seems a better choice than other PM3-based QM/MM approaches, at least for studying FAAH-catalyzed reactions.

The present calculations show that the collapse of the TI follows a concerted reaction mechanism, where Lys142 and Ser217 cooperate in the protonation of the leaving group heteroatom (nitrogen for OA, oxygen for OME). Protonation of the leaving group is identified as the key event in acylation for both OA and OME, a finding that provides a theoretical explanation for the remarkable ability of FAAH to hydrolyze amides faster than esters.

Taken together, these findings indicate that SCC-DFTB/CHARMM27 QM/MM calculations provide good results for FAAH, and will be useful to characterize the catalytic mechanisms of other related enzymes. Due to its fair accuracy and limited computational cost, the SCC-DFTB/CHARMM27 potential will be also useful for free-energy simulations based on umbrella sampling molecular dynamics [44] or on other enhanced sampling approaches [1, 5].

Acknowledgments AJM and EC thank the Engineering and Physical Science Research Council for support. AJM is an Engineering and Physical Science Research Council Leadership Fellow. JS thanks the Royal Thai Government for funding.

References

1. Lonsdale R, Ranaghan KE, Mulholland AJ (2010) Computational enzymology. Chem Commun 46:2354–2372
2. Cavalli A, Carloni P, Recanatini M (2006) Target-related applications of first principles quantum chemical methods in drug design. Chem Rev 106:3497–3519
3. Field MJ, Bash PA, Karplus M (1990) A combined quantum mechanical and molecular mechanical potential for molecular dynamics simulations. J Comput Chem 11:700–733
4. Warshel A (2003) Computer simulations of enzyme catalysis: methods, progress, and insights. Annu Rev Biophys Biomol Struct 32:425–443
5. Senn HM, Thiel W (2009) QM/MM methods for biomolecular systems. Angew Chem Int Ed Engl 48:1198–1229
6. Friesner RA, Guallar V (2005) Ab initio quantum chemical and mixed quantum mechanics/molecular mechanics (QM/MM) methods for studying enzymatic catalysis. Annu Rev Phys Chem 56:389–427
7. Claeyssens F, Harvey JN, Manby FR, Mata RA, Mulholland AJ, Ranaghan KE, Schütz M, Thiel S, Thiel W, Werner HJ (2006) High accuracy computation of reaction barriers in enzymes. Angew Chem Int Ed Engl 45:6856–6859
8. Mulholland AJ (2007) Chemical accuracy in QM/MM calculations on enzyme-catalysed reactions. Chem Cent J 1:1–19
9. Lodola A, Sirirak J, Fey N, Rivara S, Mor M, Mulholland AJ (2010) Structural fluctuations in enzyme-catalyzed reactions:

determinants of reactivity in fatty acid amide hydrolase from multivariate statistical analysis of quantum mechanics/molecular mechanics paths. J Chem Theor Comput 6:2948–2960
10. Ridder L, Mulholland AJ (2003) Modeling biotransformation reactions by combined quantum mechanical/molecular mechanical approaches: from structure to activity. Curr Top Med Chem 3:1241–1256
11. Elstner M, Porezag D, Jungnickel G, Elsner J, Haugk M, Frauenheim T, Suhai S, Seifert G (1998) Self-consistent-charge density-functional tight-binding method for simulations of complex materials properties. Phys Rev B 58:7260–7268
12. Otte N, Scholten M, Thiel W (2007) Looking at self-consistent-charge density functional tight binding from a semiempirical perspective. J Phys Chem A 111:5751–5755
13. Elstner M (2006) The SCC-DFTB method and its application to biological systems. Theor Chem Acc 116:316–325
14. Xu D, Guo H, Cui Q (2007) Antibiotic binding to dizinc β-lactamase L1 from *Stenotrophomonas maltophilia*: SCC-DFTB/CHARMM and DFT studies. J Phys Chem A 111:5630–5636
15. Cui Q, Elstner M, Kaxiras E, Frauenheim T, Karplus M (2001) A QM/MM implementation of the self-consistent charge density functional tight binding (SCC-DFTB) method. J Phys Chem B 105:569–585
16. Seabra G, Walker RC, Elstner M, Case DA, Roitberg AE (2007) Implementation of the SCC-DFTB method for hybrid QM/MM simulations within the Amber molecular dynamics package. J Phys Chem A 26:5655–5664
17. Riccardi D, Schaefer P, Yang Y, Yu H, Ghosh N, Prat-Resina X, König P, Li G, Xu D, Guo H, Elstner M, Cui Q (2006) Development of effective quantum mechanical/molecular mechanical (QM/MM) methods for complex biological processes. J Phys Chem B 110:6458–6469
18. Lodola A, Mor M, Hermann JC, Tarzia G, Piomelli D, Mulholland AJ (2005) QM/MM modelling of oleamide hydrolysis in fatty acid amide hydrolase (FAAH) reveals a new mechanism of nucleophile activation. Chem Commun 35:4399–4401
19. Lodola A, Mor M, Rivara S, Christov C, Tarzia G, Piomelli D, Mulholland AJ (2008) Identification of productive inhibitor binding orientation in fatty acid amide hydrolase (FAAH) by QM/MM mechanistic modelling. Chem Commun 2:214–216
20. Piomelli D (2003) The molecular logic of endocannabinoid signalling. Nat Rev Neurosci 4:873–884
21. Piomelli D, Tarzia G, Duranti A, Tontini A, Mor M, Compton TR, Dasse O, Monaghan EP, Parrott JA, Putman D (2006) Pharmacological profile of the selective FAAH inhibitor KDS-4103 (URB597). CNS Drug Rev 12:21–38
22. Lodola A, Mor M, Zurek J, Tarzia G, Piomelli D, Harvey JN, Mulholland AJ (2007) Conformational effects in enzyme catalysis: reaction via a high energy conformation in fatty acid amide hydrolase. Biophys J 92:L20–L22
23. Tubert-Brohman I, Acevedo O, Jorgensen WL (2006) Elucidation of hydrolysis mechanisms for fatty acid amide hydrolase and its Lys142Ala variant via QM/MM simulations. J Am Chem Soc 128:16904–16913
24. Brooks BR, Bruccoleri RE, Olafson BD, States DJ, Swaminathan S, Karplus M (1983) CHARMM: a program for macromolecular energy, minimization, and dynamics calculations. J Comput Chem 4:187–217
25. McKinney MK, Cravatt BF (2005) Structure and function of fatty acid amide hydrolase. Annu Rev Biochem 74:411–432
26. MacKerell AD Jr, Bashford D, Bellott M, Dunbrack RL Jr, Evanseck JD, Field MJ, Fischer S, Gao J, Guo H, Ha S, Joseph-McCarthy D, Kuchnir L, Kuczera K, Lau FTK, Mattos C, Michnick S, Ngo T, Nguyen DT, Prodhom B, Reiher WE III, Roux B, Schlenkrich M, Smith JC, Stote R, Straub J, Watanabe M, Wiorkiewicz-Kuczera J, Yin D, Karplus M (1998) All-atom empirical potential for molecular modeling and dynamics studies of proteins. J Phys Chem B 102:3586–3616
27. Yin D, MacKerell AD Jr (1998) Combined ab initio/empirical approach for the optimization of Lennard–Jones parameters. J Comput Chem 19:334–338
28. Neria E, Fischer S, Karplus M (1996) Simulation of activation free energies in molecular systems. J Chem Phys 105:1902–1921
29. Shaw KE, Woods CJ, Mulholland AJ (2010) Compatibility of quantum chemical methods and empirical (MM) water models in quantum mechanics/molecular mechanics liquid water simulations. J Phys Chem Lett 1:219–223
30. Lodola A, Mor M, Sirirak J, Mulholland AJ (2009) Insights into the mechanism and inhibition of fatty acid amide hydrolase from quantum mechanics/molecular mechanics (QM/MM) modelling. Biochem Soc Trans 37(Pt 2):363–367
31. Bracey MH, Hanson MA, Masuda KR, Stevens RC, Cravatt BF (2002) Structural adaptation in a membrane enzyme that terminates endocannabinoid signaling. Science 298:1793–1796
32. Brooks CL, Karplus M (1989) Solvent effects on protein motion and protein effects on solvent motion. Dynamics of the active site region of lysozyme. J Mol Biol 208:159–181
33. Mulholland AJ, Richards WG (1997) Acetyl-CoA enolization in citrate synthase: a quantum mechanical/molecular mechanical (QM/MM) study. Proteins 27:9–25
34. Eurenius KP, Chatfield DC, Brooks BR, Hodoscek M (1996) Enzyme mechanisms with hybrid quantum and molecular mechanical potentials. I. Theoretical considerations. Int J Quantum Chem 60:1189–1200
35. Hermann JC, Hensen C, Ridder L, Mulholland AJ, Höltje HD (2005) Mechanisms of antibiotic resistance: QM/MM modeling of the acylation reaction of a class A beta-lactamase with benzylpenicillin. J Am Chem Soc 127:4454–4465
36. Hermann JC, Ridder L, Höltje HD, Mulholland AJ (2006) Molecular mechanisms of antibiotic resistance: QM/MM modelling of deacylation in a class A beta-lactamase. Org Biomol Chem 4:206–210
37. Labar G, Michaux C (2007) Fatty acid amide hydrolase: from characterization to therapeutics. Chem Biodivers 4:1882–1902
38. McKinney MK, Cravatt BF (2003) Evidence for distinct roles in catalysis for residues of the serine-serine-lysine catalytic triad of fatty acid amide hydrolase. J Biol Chem 278:37393–37399
39. Ahn K, McKinney MK, Cravatt BF (2008) Enzymatic pathways that regulate endocannabinoid signaling in the nervous system. Chem Rev 108:1687–1707
40. van der Kamp MW, Mulholland AJ (2008) Computational enzymology: insight into biological catalysts from modelling. Nat Prod Rep 6:1001–1014
41. Mileni M, Garfunkle J, Ezzili C, Kimball FS, Cravatt BF, Stevens RC, Boger DL (2010) X-ray crystallographic analysis of α-ketoheterocycle inhibitors bound to a humanized variant of fatty acid amide hydrolase. J Med Chem 53:230–240
42. Klähn M, Braun-Sand S, Rosta E, Warshel A (2005) On possible pitfalls in ab initio quantum mechanics/molecular mechanics minimization approaches for studies of enzymatic reactions. J Phys Chem B 109:15645–15650
43. Garcia-Viloca M, Gao J, Karplus M, Truhlar DG (2005) How enzymes work: analysis by modern rate theory and computer simulations. Science 303:186–195
44. Bowman AL, Ridder L, Rietjens IM, Vervoort J, Mulholland AJ (2007) Molecular determinants of xenobiotic metabolism: QM/MM simulation of the conversion of 1-chloro-2,4-dinitrobenzene catalyzed by M1-1 glutathione *S*-transferase. Biochemistry 46:6353–6363